Isotacticity effect on crystallization and melting in polypropylene fractions: 3. Overall crystallization and melting behaviour

James J. Janimak, Stephen Z. D. Cheng* and Anqiu Zhang
Institute and Department of Polymer Science, College of Polymer Science and Polymer Engineering, The University of Akron, Akron, OH 44325-3909, USA

and Eric T. Hsieh
Research and Development, Phillips Petroleum Company, Bartlesville, OK 74004, USA
(Received 5 September 1990; revised 3 December 1990; accepted 26 December 1990)

A set of polypropylene (PP) fractions with similar molecular masses and molecular mass distributions but different isotacticities have been investigated and their overall crystallization and crystal melting behaviours determined by differential scanning calorimetry and time resolved small-angle X-ray scattering experiments. The observations indicate that when the supercooling is high ($\Delta T > 48$ K), only poor and imperfect crystals can form, which are continuously annealed to more perfect crystals upon heating after isothermal crystallization. On the other hand, below $\Delta T = 48$ K, two different crystal morphologies are recognized with their own crystallization kinetics and thermal stabilities. The Avrami treatment for the overall crystallization kinetics of these PP fractions generally reveals a low Avrami exponent (n) compared with the literature data. The overall crystallization and crystal melting behaviour can be correlated to the crystal morphology change with supercooling, in particular to the 'cross-hatching' lamellar phenomenon uniquely observed in the case of PP. The isotacticity effect on the overall crystallization processes and melting behaviour are also focused upon.

(Keywords: crystal melting; crystal morphology; heat of fusion; isotacticity; kinetics; melting temperature; overall crystallization; polypropylene; thermodynamic stability)

INTRODUCTION

The overall crystallization kinetics of isotactic polypropylene (i-PP) has been extensively studied by dilatometry, microscopy, calorimetry, infra-red spectroscopy and wide-angle X-ray diffraction methods during the last three decades. These studies all showed that the overall crystallization of i-PP can achieve relatively high percentages of the maximum crystallinity, and can be best described by an Avrami expression over the wide isothermal crystallization temperature range[1-21]. Exponents of between $n = 3$ and $n = 4$ were found in most of the experiments. Furthermore, Majer[6] observed that different thermal histories in the melt may lead to a change of the Avrami exponent. By applying a two-stage crystallization model[22,23], Hoshino *et al.*[11] found a reasonable description for results of X-ray experiments using an Avrami exponent $n_1 = 3.9$ for primary crystallization, and $n_2 = 1.8$ for secondary crystallization. Other values biased towards an Avrami exponent of $n = 2$, instead of $n = 3$, were found by calorimetry and analysed by Godovskii and Slonimskii[12] and Godovskii[13] in terms of a possible different nucleation mechanism. On the other hand, Pratt and Hobbs[16] determined the Avrami exponent of $n = 3$ by differential scanning calorimetry (d.s.c.) and depolarization microscopy. Carfagna *et al.*[19] showed that in the presence of unmelted materials, namely seeds, the n values ranged from 0.5 to 1.6, which differs from typical values[20,21] of $n = 3$. When the melt is initially heated to 473 K and above, for suitable crystallization temperatures, the Avrami exponent increases to $n = 4$, indicating a change from an athermal to thermal nucleation[19]. With increasing the seed concentration (seed crystallinity percentage), the Avrami exponent n decreases. Low Avrami exponents were also found in the crystallization of polyethylene when unmelted materials were present[21].

The melting behaviour of i-PP crystallized from the melt has been a complicated issue for quite some time. This is because the melting processes are affected not only by molecular mass and molecular mass distribution, but also by different configurations (isotacticity and head-to-tail sequences) and different crystal structures (α, β and γ forms). Equilibrium thermodynamic properties of i-PP are still somewhat uncertain, in particular, the equilibrium melting temperature of the α form in i-PP has been reported in a range between 458.2 K and 481.2 K. Two sets of data are presented: at the lower end of this temperature range in the vicinity of 458.2–460.7 K are the reported data of Krigbaum and Uematsu[24] (459.2 ± 2 K), Miller and Seeley[25] (459.2 K), Kamide and Toyama[26] (460.7 K), Martuscelli *et al.*[20] (458.0 K), Bu *et al.*[27] (460.7 K) and Cheng *et al.*[28]; at the higher end of this range an equilibrium melting

* To whom correspondence should be addressed

0032-3861/92/040728-08

temperature of around 481.2 K has been extrapolated by Fatou[29]. Samuels[30] has found that in i-PP fibres multiple melting peaks arise when a certain minimum orientation of the non-crystallizable chains is achieved. The high temperature melting peak can be extrapolated *versus* chain orientation along the fibre direction to an ultimate melting point for fully oriented chains of 493.2 K. The low temperature melting peak yields an extrapolated value of 458.2 K.

The establishment of the heat of fusion of i-PP also seems to be difficult. Literature data[31] range from 2.65 to 10.9 kJ mol^{-1}. The data obtained from calorimetry are averaged from five data sources and yield a value[31] of 6.9 $\pm$ 0.8 kJ mol^{-1}, while data from melting temperature depression due to the effect of a diluent generate a higher value for the heat of fusion[24,32] (9.1 $\pm$ 1.6 kJ mol^{-1}). A value of 8.7 $\pm$ 1.6 kJ mol^{-1} was proposed recently[27], which was indirectly supported by analyses of microhardness[33] and calculations[27] of residual entropy of amorphous i-PP at 0 K.

Experimentally observed melting behaviour of metastable i-PP crystals commonly shows multiple melting peaks. The appearance of this phenomenon has been attributed to such factors as two different crystal structures[3,34–36], two different crystal sizes[30] and recrystallization and perfection during heating[37]. Recently, it was reported that double melting peaks may be attributed to the recrystallization of less ordered α_1 form with a random distribution of up and down chain packing with methyl groups to a more ordered α_2 form with a well-defined deposition of up and down helices in the unit cell[38–40]. This process of ordering (α_1 to α_2) transition at crystallization temperatures in excess of 420 K leads to a continuous change from one form to the next.

In this paper, we attempt to correlate the overall crystallization with melting behaviour through the knowledge of crystal morphology for a set of polypropylene (PP) fractions with similar molecular mass and molecular mass distributions, but different isotacticities. Combined with our previous studies on their thermodynamic properties, linear crystal growth rates and morphologies[41,42], we hope to achieve a better understanding of crystallization and melting behaviour of these PP fractions.

EXPERIMENTAL

Samples and materials

The PP fractions studied have been designated as PP(X-20), PP(Y-17), PP(Y-9), PP(X-6) and PP(X-3). Detailed information about their molecular masses, molecular mass distributions, isotacticities and equilibrium thermodynamic properties are given in *Table 1*. The structure analysis has been described previously[41,42].

The dried PP samples were ready for d.s.c. measurements with a typical sample mass of 0.5–1.0 mg. The weights of the reference and sample pans were controlled to within $\pm$0.002 mg. The PP samples were enclosed in hermetic aluminium pans. All d.s.c. experiments were carried out under a dry nitrogen gas purge of flow rates 40–60 ml min^{-1}. The dried PP fractions of about 40 mg each were put into aluminium cups for small-angle X-ray scattering (SAXS) measurements. The samples were melted on a hot plate in vacuum at 478 K for 5 min and cooled to room temperature before experiments.

Instrumentation and experiments

A DuPont 9900 thermal analysis system was used for d.s.c. measurements and the isothermal crystallization exotherm of the PP fractions was analysed. The samples were heated to 20 K above their respective melting temperatures (see *Table 1*) on a hot stage and held there for 5 min. The samples were then quickly shifted to the d.s.c. cell where a predetermined crystallization temperature, T_c, was maintained. The exothermic processes were recorded, and then integrated at various crystallization times, t_c. At high crystallization temperatures where the crystallization processes are slow, instead of recording the exothermic processes with respect to time, the isothermal crystallization was interrupted at various crystallization times. They were then heated to 20 K above their respective melting temperatures without prior cooling. The endothermic peaks were used for the kinetic analyses. In order to study the thermal history effect on crystallization, the samples were heated to different temperatures in the melt, as well as different residence times at these temperatures. The selected residence temperatures were 1 K, 10 K and 40 K above the respective melting temperatures (*Table 1*), and the selected times were 1 min, 10 min and 20 min. The d.s.c. was calibrated according to the standard procedures.

SAXS experiments were conducted on a Cu K_α X-ray source generated by a Rigaku 12 kW rotating anode. The X-ray beam was monochromatized with a graphite crystal. A SAXS goniometer was used with a 50 cm vacuum chamber and a positional sensitive detector (Braun OED 5 cm) attached to the end of the goniometer. Lorentz corrections of the SAXS data were conducted by multiplying the intensity, I (counts per second), with s^2 ($s = 2\sin\theta/\lambda$, where λ is the wavelength of the X-ray, 1.54178 Å). A hot stage was attached on the sample holder. For isothermal measurements, thermal treatments of the samples were the same as described in the d.s.c. experiments.

Table 1 Molecular characteristics and thermal properties of the PP fractions

Assignment	$M_w \times 10^{-3}$	M_w/M_n	Isotacticity	T_m (K)[a]	ΔH_f (kJ mol^{-1})[a]
PP(X-20)	202	2.6	0.988	457.0	8.68
PP(Y-17)	159	2.3	0.978	456.0	8.66
PP(Y-9)	189	3.0	0.953	453.4	8.61
PP(X-6)	209	1.8	0.882	446.2	8.47
PP(X-3)	190	1.6	0.787	436.2	8.28

[a]Data taken from references 41 and 42

RESULTS

Overall crystallization

Typical d.s.c. melting traces for the fraction PP(X-6) are shown in *Figure 1*. The sample was crystallized at 400.2 K, corresponding to a supercooling of approximately 46 K, for different crystallization times. Two endothermic peaks can be clearly distinguished. With increasing time, both peaks develop with their own kinetics. All other PP fractions exhibit similar double melting peak endotherms as shown for PP(X-6) in *Figure 1*. This double melting behaviour appeared wih greater clarity in the lower isotactic PP fraction and was extensive over the temperature range studied. The experimental heats of fusion for these fractions have been converted to plots of volume fraction crystallinity v^c (ρ_c, ρ_a and Δh_f are quoted from references 41 and 43).

Figure 2 shows the Avrami plot based on the data from *Figure 1* for PP(X-6). The Avrami exponents of crystallization for the two melting peak materials are slightly different. This has been denoted as $n_1(h)$ and $n_1(l)$ for the high and low melting peak materials, respectively, in the initial stages of crystallization with Avrami exponent n_1. The Avrami exponent for the low melting peak material in this case is found to be $n_1(l) = 1.86$ while the Avrami exponent, $n_1(h)$, is 1.36. The overall Avrami exponent n_1 has also been analysed from the records of the exothermic crystallization peak with time at this crystallization temperature. The value for the Avrami exponent of n_1, which is a combined contribution of the low and high melting peak materials, is found to be $n_1 = 2.0$ for PP(X-6). In general, the Avrami exponents for these fractions are between 1.8 and 3.2 over the crystallization temperature range studied. A tendency of increasing values of n with decreasing supercooling is apparent. At a constant supercooling, on the other hand, this value decreases with isotacticity.

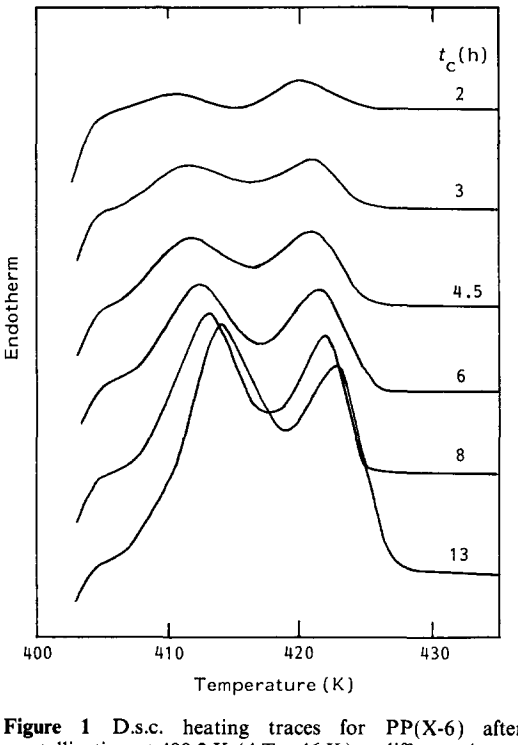

Figure 1 D.s.c. heating traces for PP(X-6) after isothermal crystallization at 400.2 K ($\Delta T = 46$ K) at different times without prior cooling

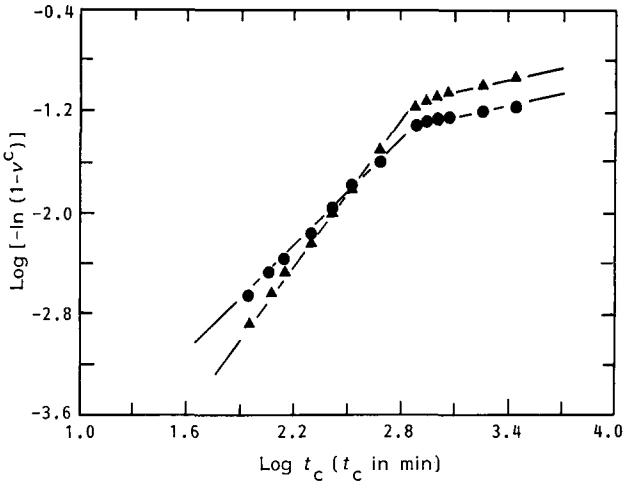

Figure 2 Avrami plots of degree of crystallinities for both low (▲) and high (●) melting peak developments with time for PP(X-6) crystallized at 400.2 K. Data are from *Figure 1*

Figure 2 also shows that at approximately the same crystallization time, a secondary crystallization process is observed in each of the two cases. However, the levels of crystallinity where these secondary crystallization processes start for the low and high melting peak materials are different. In the case of the low melting peak material, the volume fraction crystallinity approaches approximately 25% prior to the initiation of the secondary crystallization process. This is contrasted with 14% volume fraction crystallinity attained for the high melting peak materials. After approximately 13 h of crystallization time at $T_c = 400.2$ K for the above-mentioned fraction, the secondary crystallization process is initiated. This phenomenon is recognized by the distinct change in slope as shown in *Figure 2*. The Avrami exponent of $n_2(l)$ and $n_2(h)$ for both low and high melting peak materials have been found to be very small, in the range 0.2–0.4. Kinetic data for PP(Y-17), PP(Y-9) and PP(X-3) are shown in *Figures 3a–c*, and are represented in the form of Avrami plots based on the data of the exothermic crystallization processes. With increasing isothermal crystallization temperature, one finds that the Avrami exponent n_1 slightly increases while the intercept log$K$ decreases. It has been found that when the volume fraction crystallinity reaches 25% for PP(X-3), 39% for PP(X-6), 43% for PP(Y-9), 53% for PP(Y-17) and 65% for PP(X-20) at the same degree of supercooling, the secondary crystallization process is initiated which leads to a gentler increase in the Avrami plots (*Figures 2* and *3*).

Values of n_1 for the initial stage of crystallization for these PP fractions also appear to be independent of melt residence temperature and time as shown in *Figure 4*. PP(Y-9) fraction was kept in the molten state at different residence temperatures (1 K and 40 K above its melting temperature) and different residence times (1 min, 10 min and 20 min) before it was crystallized at 400.2 K. The crystallization kinetic data all fall onto the same line within a margin of ±5% error. Of particular interest is the time at which the transition between the different crystallization processes occurs, which for these fractions corresponds to the times of spherulitic impingement (spherulitic morphology as observed from polarized light microscopy[42]). It is also noted that at the spherulite impingement times, these fractions exhibit

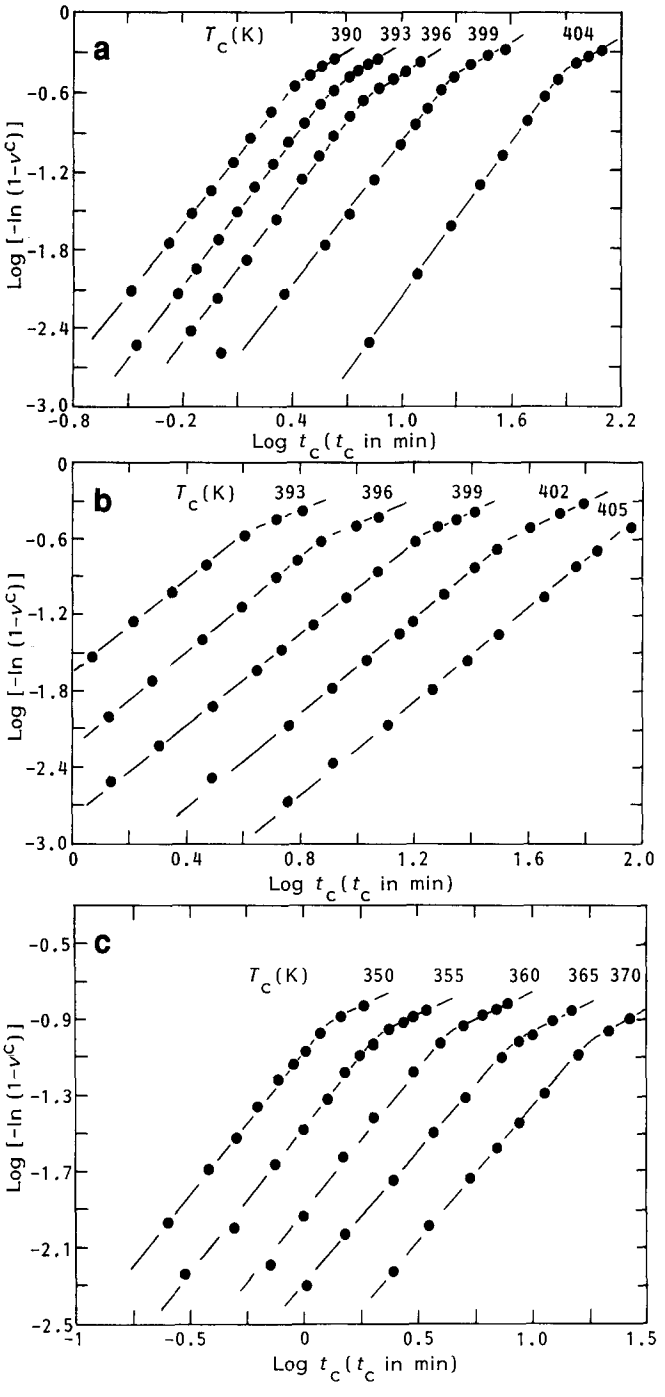

Figure 3 Avrami plots between log[-ln(1-v^c)] and log t_c for (a) PP(Y-17), (b) PP(Y-9) and (c) PP(X-3)

different crystallinities. This would seem to indicate that the secondary crystallization process associated with n_2 proceeds on a finer textural scale within spherulites.

Changes in lamellar long spacing during crystallization

Time resolved SAXS experiments for these PP fractions crystallized at different temperatures lead to the observation of changes in lamellar long spacing with time. *Figures 5a* and *b* show the SAXS curves for PP(X-20) crystallized at 424.2 K ($\Delta T = 36$ K), and PP(X-6) crystallized at 390.2 K ($\Delta T = 56$ K), respectively, as examples. For all five fractions, we have carried out isothermal crystallization SAXS measurements in the temperature ranges equivalent to the study in overall crystallization kinetics and crystal melting (supercooling range between 90 K and 36 K). In the whole temperature range studied, disregarding different isotacticities of the samples, it is interesting to note that at short crystallization times the first scattering peak from SAXS observations generally shows relatively large lamellar long spacings. With increasing time, and at low crystallization temperatures as shown in *Figure 5b*, a decrease of the spacing is evident by a broadening of the scattering peak. This leads to a gradual decrease of the lamellar long spacings. In the case shown in *Figure 5b*, the initial lamellar long spacing is 28.9 nm. After complete crystallization, it decreases to 28.0 nm. On the other hand, at high crystallization temperatures (*Figure 5a*), the appearance of the second scattering peak with smaller lamellar long spacing (30.4 nm) appears

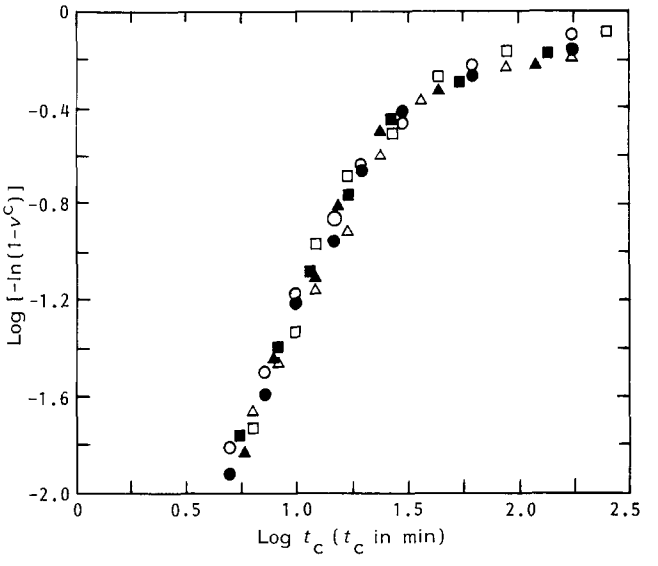

Figure 4 Avrami plots of the isothermal crystallization of PP(Y-9) at $T_c = 400.2$ K for different residence temperatures (solid symbols, 459 K; open symbols, 498 K) and times: ○, 1 min; △, 10 min; □, 20 min

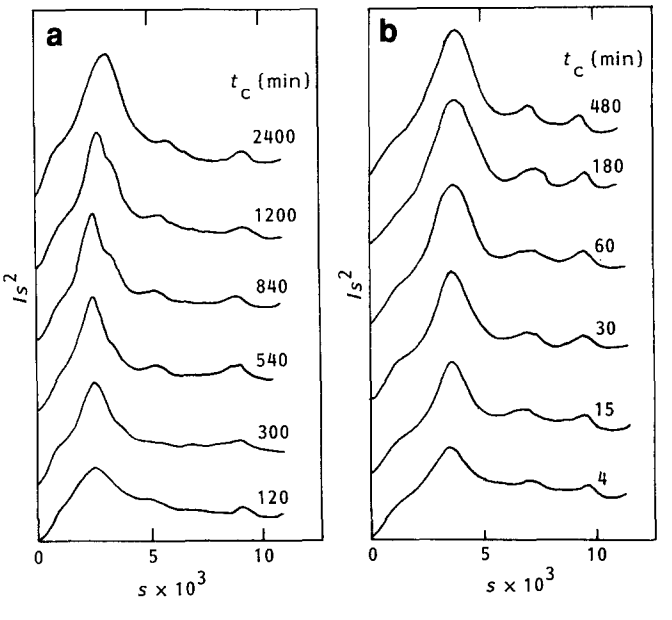

Figure 5 Time resolved SAXS curves for isothermal crystallizations of (a) PP(X-20) at $T_c = 442.2$ K ($\Delta T = 36$ K); (b) PP(X-6) at $T_c = 390.2$ K ($\Delta T = 56$ K)

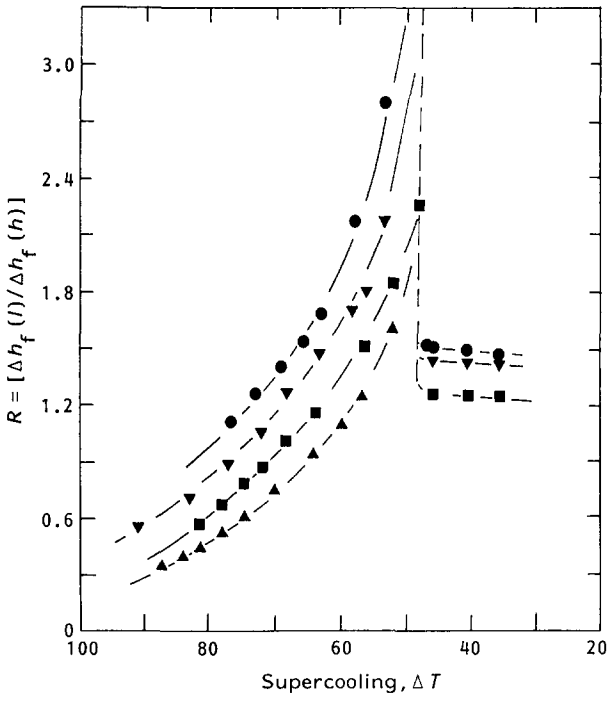

Figure 6 Relationships between R $[\Delta h_f(l)/\Delta h_f(h)]$ and supercooling (ΔT) for PP fractions crystallized in a supercooling range between 90 K and 36 K. ●, PP(Y-17); ▼, PP(Y-9); ■, PP(X-6); ▲, PP(X-3)

much later in comparison with the first scattering peak (40.3 nm). The two peaks merge only after prolonged times where, again, the secondary crystallization process starts. The difference between two lamellar long spacings thus increases with crystallization temperature, as shown in *Figures 5a* and *b*.

Crystal melting

As described above, two melting peaks can be observed during heating after isothermal crystallization. At high supercooling ($\Delta T > 48$ K) the low melting peak is generally broad, and usually starts only a few degrees above the crystallization temperature. The high melting peak is, however, quite sharp and relatively narrow. It is interesting to pursue the change in heats of fusion for these two melting peak materials with supercooling at a heating rate of 10 K min^{-1}. *Figure 6* shows that in a supercooling range of about 60 K the ratio, R, of $\Delta h_f(l)/\Delta h_f(h)$, changes with supercooling. Here $\Delta h_f(l)$ and $\Delta h_f(h)$ represent the heats of fusion of the low melting peak and the high melting peak materials, respectively. For these fractions, the parameter R initially increases with decreasing supercooling and reaches a maximum. As much as a factor of two exists between the lowest and the highest isotacticity fraction at a constant supercooling in this region. Further increase in crystallization temperature reduces the value of R (see *Figure 6*). The crystallization temperature where the maximum R appears is different for each fraction. Nevertheless, the degree of supercooling which corresponds to these temperatures is essentially the same: 48 ± 2 K. Furthermore, below $\Delta T = 48$ K, the absolute value of R seems to be still dependent upon isotacticity. For PP(X-20) and PP(Y-17), with higher isotacticity content, R is generally greater when compared with those fractions of lower isotacticity content.

To study the relationship between these two melting peak materials, different heating rates were applied for these fractions crystallized at constant supercooling, and *Figure 7* shows linear relationships between the parameter R and logarithmic heating rate for four fractions crystallized at $\Delta T = 56$ K. Surprisingly enough, the value of R decreases with increasing heating rate, indicating that a higher heat of fusion for the high melting peak material is observed at a faster heating rate. Again, the change in absolute value of R accelerates with decreasing isotacticity. For each particular fraction, on the other hand, this change slows down with increasing crystallization temperature (or decreasing supercooling). Below $\Delta T = 48$ K the change of R with heating rate vanishes or even reverses, i.e. the value of R increases with heating rate, as illustrated in *Figure 8* for PP(Y-17) fraction.

Figure 9 shows the relationship between the melting and crystallization temperatures of PP(Y-17) and PP(X-3), as examples. For all the fractions two melting peaks are observed, and their corresponding melting temperatures are designated to be $T_m(l)$ for the low melting peak temperature, and $T_m(h)$ for the high melting peak temperature, respectively. It is clear that $T_m(l)$

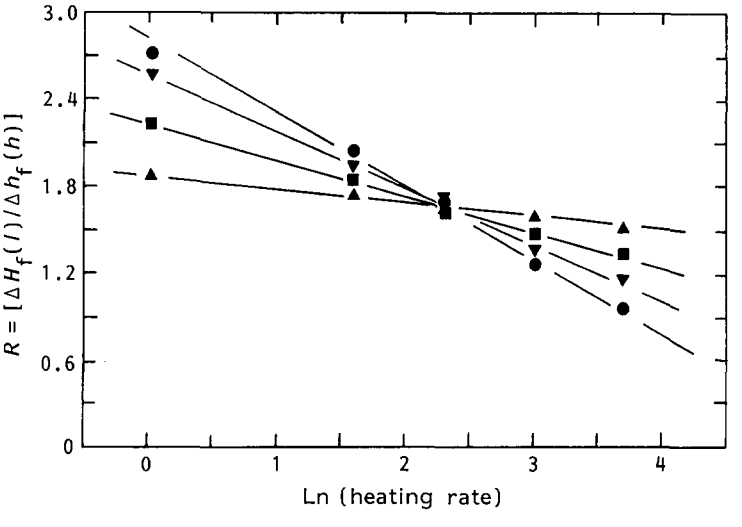

Figure 7 Relationships between R and logarithmic heating rate for PP fractions crystallized at $\Delta T = 56$ K. ▲, PP(Y-17); ■, PP(Y-9); ▼, PP(X-6); ●, PP(X-3)

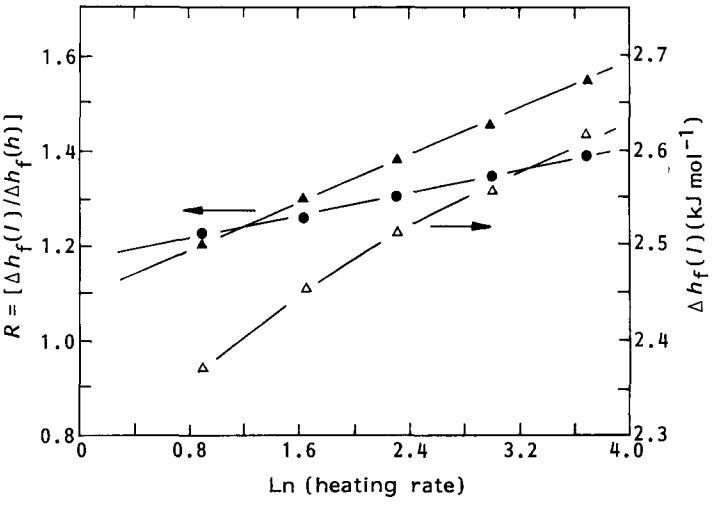

Figure 8 Relationships between R and logarithmic heating rate for PP(Y-17) crystallized at $\Delta T = 46$ K (△, ▲) and $\Delta T = 36$ K (●). Changes of $\Delta h_f(l)$ with heating rate are also included

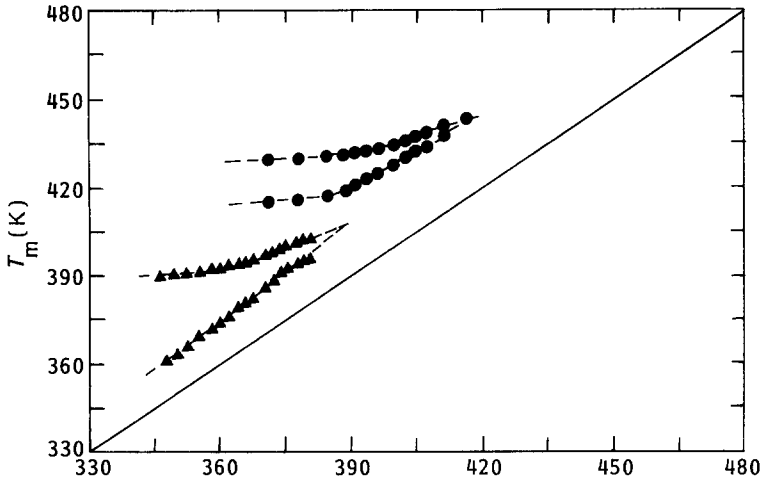

Figure 9 Relationships between T_m and T_c for PP(Y-17) (●) and PP(X-3) (▲)

increases with crystallization temperature at a faster rate than $T_m(h)$ in the temperature range studied. Both peaks may eventually merge at certain supercoolings. Decreasing the supercooling further leads to the reappearance of double melting peaks.

DISCUSSION

The major concern in this paper is the establishment of a relationship between overall crystallization and crystal melting behaviour with prior knowledge of the crystal morphology. However, a new proof of the equilibrium melting temperature of i-PP is discussed first.

Recently, a set of PP oligomers with very narrow molecular mass distributions and high isotacticities was synthesized[44]. The melting temperatures of these oligomers were measured after synthesis and precipitation from solution. The d.s.c. heating traces showed that their melting peaks were quite narrow and sharp. Also, premelting behaviour was apparent in these oligimers[45]. We estimate that up to a molecular mass of 2040 (extended chain length of 10.5 nm) extended chain crystals can be formed. Based on Pino's data[44] and our own, one can extrapolate the melting temperature of i-PP to an infinite chain length. If a linear relationship between T_m and $1/x$ is applied, the extrapolated value is 457.4 K, where x is the degree of polymerization. When a more complicated function is used, it fits to

$$T_m = 460.8(x - 4.893)/(x + 0.807 \ln x - 3.109) \quad (1)$$

with the equilibrium melting temperature of 460.8 K. The latter extrapolation yields a better fit with a standard deviation of 0.72%. This type of extrapolation leads to a value at the lower side of the reported equilibrium melting temperature range of i-PP[24–28]. Many years ago, Flory proposed a thermodynamic theory to describe equilibrium melting temperatures for pure oligomeric compounds and fractions[46]. However, it is difficult to apply his theory to illustrate this case due to unknown surface free energy contributions and premelting phenomena on the chain end surfaces, as indicated recently in the case of *n*-alkanes and low molecular mass polyethylene fractions[47].

Turning to our major concern, what are the causes of the multiple melting peaks? From *Figure 7* it is evident that the observations reported here contrast with those reported in the literature[37,48–51]. To explain the phenomenon shown in *Figure 7*, one expects that crystals grown during isothermal crystallization at high supercoolings ($\Delta T > 48$ K) are small and imperfect, and their metastabilities are low. Melting temperatures of these crystals should not be very much above their crystallization temperatures. After isothermal crystallization, a heating process without prior cooling perfects the crystals continuously, which leads to a higher melting temperature. However, as soon as these imperfect crystals are annealed, further perfections become increasingly difficult. Since a slower heating rate allows the imperfect crystals to be annealed over a relatively longer period of time compared with faster rates, the crystals can consequently attain a certain degree of perfection, and thus gain a certain degree of stability (a decrease of Gibbs free energy). As a result, they maintain that metastability for relatively long times and melt at lower temperatures. On the other hand, a faster heating rate may not allow much time to anneal these crystals, while the imperfect crystals, at least part of them, may easily be reorganized and/or recrystallized at higher temperatures to form more stable crystals which have high melting peaks. The experimental evidence is shown in *Figure 6*, where the values of R increase with decreasing ΔT. This explanation is also supported by the observation in broadness of the low melting peaks, by the linear relationship between R and logarithmic heating rate, from SAXS measurements (*Figure 5b*) where a relatively broad scattering peak is observed, and by transmission electron microscopy observations where both radial and tangential lamellae have the same lamellar thicknesses[42]. This indicates that in this supercooling region, the multiple melting peaks observed are caused by perfection and/or recrystallization of imperfect crystals initially grown during isothermal crystallization. Interestingly enough, as illustrated in *Figure 7*, the change of R with logarithmic heating rate decreases with increasing isotacticity. On the other hand, at a constant supercooling the value of R increases with the isotacticity (*Figure 6*). Namely, the heat of fusion attributed to the low melting peak materials increases with the isotacticity. This reveals that imperfect crystals with a relatively high isotacticity are less easy to anneal further compared with those with low isotacticity after they reach a certain metastability.

From *Figure 6*, it is evident that a change in the value of R at $\Delta T = 48$ K for all these fractions indicates that the crystal melting behaviour does indeed change around this supercooling. This can also be observed from *Figure 9*. The merger of two melting peak temperatures for these fractions is also approached in this vicinity of supercooling. When $\Delta T < 48$ K, it is found that the ratio R is almost independent or slightly increases with heating rate (*Figure 8*). Two primary crystallization processes can be observed (*Figures 1* and *2*). This can be understood by the fact that two populations of crystals exist, with different thermal metastabilities in this supercooling region. From the SAXS measurements, two scattering peaks are clearly distinct, revealing two different long spacings of lamellar crystals (*Figure 5a*). The TEM study indicates that the lamellae grown along the radial direction (R lamellae) usually have a thicker lamellar thickness, compared with those grown almost perpendicular to the radial direction (T lamellae, or cross-hatching lamellae), having a thinner lamellar

thickness[42]. The quantitative thickness data obtained from the SAXS measurements correspond well to the data observed from the TEM study. Furthermore, in *Figure 6*, the value of R decreases with isotacticity. This is related to the observation from TEM where the T lamellar population decreases with isotacticity[42]. Therefore, in this supercooling region two melting peaks are attributed to the two different crystal morphologies, although annealing of the low melting peak material to the high one can still be observed. It has been reported that further decrease in supercooling will lead to a single high melting peak[37]. This indicates that the population of T lamellae decreases with supercooling, which is consistent with polarized light microscopy and TEM observations[3,42,52]. The α_1 and α_2 forms with different crystal symmetries can only be distinguished[38–40] beyond $\Delta T < 35$ K.

Besides the recognition of the two primary crystallization processes when $\Delta T < 48$ K, the Avrami exponent (n) decreases with isotacticity at a constant ΔT. This indicates that three-dimensional development of the crystal texture is influenced by isotacticity; this is consistent with the TEM observations[42]. On the other hand, a slight increase in the value of n for each fraction with decreasing supercooling when $\Delta T > 48$ K may be related to high homogeneous nucleation densities and fast crystal growth of these PP fractions. Also, in contrast to the earlier work[6,19], it is evident that no residence temperature and time effects can be observed in these PP fractions (*Figure 4*). Therefore, the relatively low Avrami exponent, which is essentially insensitive to thermal history, is not due to the number of primary nuclei present but is rather a result of the polymer characteristics. Incidentally, it is interesting to find that the change of crystal melting behaviour at $\Delta T = 48$ K for these PP fractions corresponds very well to the regime transition of II/III observed in crystal growth study[42].

It is finally worthwhile paying attention to the time resolved SAXS observations shown in *Figures 5a* and *b* since they may serve as a first step in the understanding of crystal texture development. Apparently, the development of crystal texture begins with the formation of radially elongated leading lamellar crystals, with subsequent growth between the leading lamellae. At high supercoolings compact textures have been observed from both polarized light microscopy and TEM[42]. The subsequent growth is concomitantly within these leading lamellae and usually occurs not far behind them. The lamellar long spacings for both lamellae are essentially indistinguishable. This leads to a rather broad SAXS scattering peak as observed in *Figure 5b*. At low supercoolings, more open textures appear. The subsequent growth is predominantly the 'in-filling' type. This type grows considerably later[53,54]. As a result, two distinct lamellar long spacings can be observed. The large spacing corresponds to the growth of leading lamellae, and the small spacing to growth of in-filling lamellae. The cross-hatching lamellae (T lamellae) can grow from an epitaxy either on the leading lamellae or on the in-filling lamellae. From the TEM study, two different lamellar thicknesses for both R lamellae and T lamellae have been recognized when these fractions are crystallized in this supercooling region[42]. One expects that the SAXS results shown in *Figures 5a* and *b* may represent some correlation with the development of R and T lamellae. Nevertheless, quantitative correspondences are still awaited for further experimental observations in both TEM and SAXS studies.

ACKNOWLEDGEMENTS

This work was partially supported by Exxon Educational Foundation. A fruitful discussion of the crystal melting behaviour of these PP fractions with Professor B. Wunderlich (SZDC) is also gratefully acknowledged. The PP fractions were kindly provided by the Phillips Petroleum Company, Bartlesville, OK, USA.

REFERENCES

1 von Falkai, B. and Stuart, H. A. *Kolloid Z.* 1959, **162**, 138
2 von Falkai, B. *Makromol. Chem.* 1960, **41**, 86
3 Padden Jr., F. J. and Keith, H. D. *J. Appl. Phys.* 1959, **30**, 1479
4 Marker, L., Hay, P. M., Tilley, G. P., Early, R. M. and Sweeting, O. J. *J. Polym. Sci.* 1959, **38**, 33
5 Griffith, J. H. and Ranby, B. G. *J. Polym. Sci.* 1959, **38**, 107
6 Majer, J. M. *Kunststoffe* 1960, **50**, 565
7 Magill, J. H. *Nature* 1961, **191**, 1092; Magill, J. H. *Polymer* 1962, **3**, 35
8 Limbert, F. J. and Baer, E. *J. Polym. Sci. Part A* 1963, **1**, 3317
9 Parrini, P. and Correri, G. *Makromol. Chem.* 1963, **62**, 83
10 Donald, H. J., Humes E. S. and White, L. W. *J. Polym. Sci. Part C* 1964, **6**, 93
11 Hoshino, S., Meinecke, E., Power, J., Stein, R. S. and Newman, S. *J. Polym. Sci. Part 1* 1965, **3**, 3041
12 Godovskii, Yu, K. and Slonimskii, G. L. *Polym. Sci. USSR* 1966, **8**, 441
13 Godovskii, Yu, K. *Polym. Sci. USSR* 1969, **11**, 2423
14 Binsbergen, F. L. and DeLange, B. G. M. *Polymer* 1970, **11**, 309
15 von Johnsen, U. and Spilgies, G. *Kolbid Z. Z. Polym.* 1972, **250**, 1174
16 Pratt, C. F. and Hobbs, S. Y. *Polymer* 1976, **17**, 12
17 Ishizuka, O. and Koyama, K. *Polymer* 1977, **18**, 913
18 Wlochowicz, A. and Eder, M. *Polymer* 1981, **22**, 1285
19 Carfagna, C., DeRosa, C., Guerra, G. and Petraccone, V. *Polymer* 1984, **25**, 1462
20 Martuscelli, E., Pracella, M. and Crispino, L. *Polymer* 1983, **24**, 693
21 Martuscelli, E., Pracella, M., Volpe, G. D. and Greco, P. *Makromol. Chem.* 1984, **185**, 1041
22 Zachamann, H. G. and Stuart, H. A. *Makromol. Chem.* 1960, **41**, 131
23 Fischer, E. W. *Pure Appl. Chem.* 1971, **26**, 385
24 Krigbaum, W. R. and Uematsu, I. *J. Polym. Sci. Part A* 1965, **3**, 767
25 Miller, R. L. and Seeley, E. G. *J. Polym. Sci. Polym. Phys. Edn* 1982, **20**, 2297
26 Kamide, K. and Toyama, K. *Kobunshi Kagaku* 1969, **25**, 49
27 Bu, H.-S., Cheng, S. Z. D. and Wunderlich, B. *Makromol. Chem. Rapid Commun.* 1988, **9**, 76
28 Cheng, S. Z. D., Janimak, J. J., Zhang, A.-Q. and Cheng, H. N. *Macromolecules* 1990, **23**, 298
29 Fatou, J. G. *Eur. Polym. J.* 1971, **7**, 1057
30 Samuels, R. J. *J. Appl. Polym. Sci.* 1975, **13**, 1417
31 Wunderlich, B. 'Macromolecular Physics, Crystal Melting', vol. 3, Academic, New York, 1980
32 Danusso, F. and Gianotti, G. *Eur. Polym. J.* 1968, **4**, 165
33 Balta-Calleja, F. J., Martinez Salazer, J. and Asano, T. *J. Mater. Sci. Lett.* 1988, **7**, 165
34 Keith, H. D., Padden Jr., F. J., Walter, N. M. and Wylsoff, M. W. *J. Appl. Phys.* 1959, **30**, 1485
35 Kardos, J., Christiansen, A. W. and Baer E. *J. Polym. Sci. Part A-2* 1966, **4**, 477
36 Pae, K. D. *J. Polym. Sci. Part A-2* 1968, **6**, 657; Pae, K. D. and Sauer, J. A. *J. Polym. Sci.* 1968, **12**, 1901; 1921
37 Yadav, Y. S. and Jain, P. C. *Polymer* 1986, **27**, 721

38 Guerra, G., Petraccone, V., Corradini, P., De Rosa, C., Napolitano, R. and Pirozzi, B. *J. Polym. Sci. Polym. Phys. Edn.* 1984, **22**, 1029

39 Petraccone, V., Guerra, G., De Rosa, C. and Tuzi, A. *Macromolecules* 1985, **18**, 813

40 Petraccone, V., De Rosa, C., Guerra, G. and Tuzi, A. *Makromol. Chem. Rapid Commun.* 1984, **5**, 631

41 Cheng, S. Z. D., Janimak, J. J., Zhang, A.-Q. and Hsieh, E. T. *Polymer* 1991, **32**, 648

42 Janimak, J. J., Cheng, S. Z. D., Giusti, P. A. and Hsieh, E. T. *Macromolecules* 1991, **24**, 2253

43 Wunderlich, B. 'Macromolecular Physics, Crystal Structure, Morphology, Defects', Vol. 1, Academic, New York, 1973

44 Pino, P., Cioni, P. and Wei, J. *J. Am. Chem. Soc.* 1987, **109**, 6189

45 Pino, P. personal communication with SZDC, 1989

46 Flory, P. J. *J. Phys. Chem.* 1949, **17**, 223

47 Mandelkern, L., Prasad, A., Alamo, R. G. and Stack, G. M. *Macromolecules* 1990, **23**, 3696

48 Brown, R. G. and Eby, R. K. *J. Appl. Phys.* 1964, **35**, 1156

49 Bair, H. E., Salovey, R. and Huseby, T. W. *Polymer* 1967, **8**, 9

50 Kamide, K. and Yamaguchi, K. *Makromol. Chem.* 1972, **162**, 205

51 Guerra, G., De Rosa, C., Petraccone, V. and Tuzi, A. *J. Therm. Anal.* 1985, **30**, 1537

52 Norton, D. R. and Keller, A. *Polymer* 1985, **26**, 704

53 Cheng, S. Z. D., Barley, J. S. and Giusti, P. A. *Polymer* 1990, **31**, 845

54 Heberer, D. P., Cheng, S. Z. D., Barley, J. S., Lien, S. H.-S., Bryant, R. G. and Harris, F. W. *Macromolecules* 1991, **24**, 1890